Lab on a Chip

PAPER

View Article Online
View Journal

Cite this: DOI: 10.1039/d5lc00452g

Enhancing microscale printing accuracy in LCD-based 3D printing using an immobilized release film†

Chang Tian, *[abc] Chaojie Shao,[b] Tiantian Li,[b] Wenya Tang,[b] Peiqi Wu,[b] Qian Xu,[b] Wei Li*[d] and Fen Zhang*[e]

With the development of 3D printing technology, liquid crystal display (LCD)-based 3D printing offers a cost-effective solution for microfluidic device fabrication, yet its microscale precision remains limited. The accuracy of printing molds can be improved by reducing the adhesion force between the cured resin and release film. However, the adhesion force between the LCD screen and release film and the deformation of the release film in the separation process are still ignored. Herein, we propose using an immobilized release film to enhance the printing accuracy in microscale printing for microfabrication. By applying transparent double-sided adhesive tape between the LCD screen and release film, the movement and deformation of the release film can be reduced, the vertical accuracy in the process of microscale 3D printing can be improved, and the error rate in height can be reduced from 20% to 5%. By studying the printing effect under different layer heights, it was found that when the layer height was set as 20–30 μm, the printed micromold matched the design features in both size and side structure. Moreover, microstructures less than 30 μm in width can be obtained. Besides, the reproducibility of the immobilized release film across different resins was confirmed. Furthermore, microfluidic chips used in concentration gradient generation can be obtained with a minimum cross section of 204 μm. Finally, we used the printed mold to fabricate a PDMS chip in the study of silicosis and the preventive effect of NAC in silicosis. Moreover, the mechanism of the preventive effect of NAC was studied. We believe that our fabrication technique with an immobilized release film will facilitate the development of microfluidic technology, and expand the scope and application of microfluidics in research and applications in diverse fields, such as analytical biochemistry, pharmaceuticals, and medicine.

Received 8th May 2025,
Accepted 24th June 2025

DOI: 10.1039/d5lc00452g

rsc.li/loc

Introduction

3D printing is a newly developed technology in fabrication.[1] Unlike traditional subtractive construction, 3D printing has been applied in the food industry,[2] construction industry,[3] industrial manufacturing,[4] and so on. In the field of microfabrication, complex 3D geometries can be constructed by 3D printing with fast prototyping.[5] Nowadays, there are three main 3D printing technologies commonly applied in microfluidics, *i.e.*, fused deposition modeling (FDM),[6] stereo lithography appearance (SLA),[7] and polyjet.[8] FDM technology utilizes thermoplastic materials to stack and mold the model. The FDM-based 3D printer device is cost-effective, and the model can be easily constructed. However, FDM-based 3D-printed microdevices show crucial challenges that need to be overcome, including low accuracy, low optical transparency, high surface roughness, and difficulties in creating tiny internal structures of the channels.[6,9] Polyjet-based 3D-printed microdevices can be performed with high accuracy, good optical transparency, and considerable surface roughness. Nevertheless, the post-treatment of polyjet-based 3D-printed microdevices is particularly time-consuming and tedious.[10] Moreover, the incomplete cleaning of microdevices will lead to distortion of the structure. Besides, the purchase and maintenance of polyjet-based 3D-printers costs more than hundreds of thousands of dollars, which is prohibitively expensive. Using SLA-based 3D-printing, microfluidic devices can be achieved using a laser beam to cure a photosensitive

[a] Public Health School, Anhui University of Science & Technology, Huainan, Anhui 232001, PR China. E-mail: tianchang984@nwsuaf.edu.cn
[b] Medical School, Anhui University of Science & Technology, Huainan, Anhui 232001, PR China
[c] Key Laboratory of Industrial Dust Deep Reduction and Occupational Health and Safety of Anhui Higher Education Institutes, Anhui University of Science & Technology, Huainan, Anhui 232001, PR China
[d] The First Affiliated Hospital, Anhui University of Science & Technology, Huainan, Anhui 232001, PR China. E-mail: lw07512@163.com
[e] School of Food and Bioengineering, Xuzhou University of Technology, Xuzhou, Jiangsu 221018, PR China. E-mail: zhangfen@xzit.edu.cn

† Electronic supplementary information (ESI) available: ESI is available on the website. See DOI: https://doi.org/10.1039/d5lc00452g

resin point by point. The fabricated microfluidic device is highly accurate under the control of a high-precision laser. However, the need for an SLA-based 3D-printer poses an economic barrier for researchers. Furthermore, the fabrication process is quite long due to the point-by-point printing.[11,12]

Recently, among the SLA 3D printing technologies, commercialized LCD-based 3D printers and digital light projection (DLP)-based 3D printers have attracted the attention of many groups.[13,14] The printing process can be shortened through layer-by-layer curing of the resin, which significantly reduces the printing time. However, the optical distortion caused by the complex optical path system of DLP-based printers leads to poor accuracy under high-precision printing.[15] Furthermore, the high cost and technical requirement of complex optical component design in customized DLP-3D printers hinders their further application in microfabrication.[16] In contrast, the printing accuracy and cost-effectiveness of LCD-based printers can be improved through contact exposure to a UV lamp and an LCD mask.[17] At present, the resolution of LCD screens can achieve the micron level, which is extremely attractive in microfabrication.[18] Furthermore, the production process and post-treatment are convenient, fast, non-toxic and harmless. Besides, there is no need for large space or trained technical personnel, demonstrating great potential in the field of microfluidic chip preparation.[19] Although LCD-based 3D printers have been widely used in the field of microfabrication and have shown great potential for application, there are still shortcomings in high-precision printing; in particular, size deviation is a common problem in printing.[20–23] To overcome this problem, Zhang *et al.* proposed a dimension compensation method to optimize the printing parameters and provide a straightforward post-treatment technique to ensure high-quality curing of polydimethylsiloxane (PDMS) in master molds made from photosensitive resin.[24] Although this size compensation method can correct the printing size during the printing process, the mechanism for the size differences of LCD printers was not analyzed.

During the bottom-up printing process of LCD-based printing, the separation between the cured resin and the resin tank is an important step in the layer printing process, which influences the printing quality and speed.[25] Nowadays, various materials have been investigated and applied as release films between the resin tank and LCD screen in mold printing, such as fluorinated ethylene propylene (FEP), Teflon, immiscible fluorinated oil, PDMS, and hydrogel.[26–31] FEP film offers high light transmittance, a smooth surface, and non-stick properties, which greatly improve printing success rates and have led to its widespread commercial use. However, the adhesive force between the FEP film and the cured resin is too large, which leads to failure of continuous printing and high-quality mold fabrication. To address this problem, innovative releasing techniques have been proposed to achieve rapid 3D printing. Tumbleston *et al.* proposed continuous liquid interface printing (CLIP) to create a "dead zone", which is a thin uncured liquid layer that prevents adhesion between the window and the cured resin.[32] Drawing inspiration from the peristome surface of the pitcher plant, Wu *et al.* proposed a slippery surface to maintain ultra-low adhesive energy at the interface for continuous 3D printing.[33] Wen *et al.* utilized a superamphiphobic interface to reduce adhesive forces by mimicking the surface structure of a lotus leaf.[34] The poor adhesion between the release film and the cured resin was beneficial for improving the printing efficiency and reducing the curing time. In short, by reducing the adhesion between the cured resin and the release film, the deformation of the release film in the release process can be effectively reduced, and printing accuracy can be achieved. Notably, the current research mainly focuses on the relationship between the release film and the cured resin, ignoring the changes between the LCD screen and release film. Wu *et al.* presented an extraordinarily soft hydrogel as an excellent separation interface to enable rapid printing, which is a distinct separation mechanism compared with reducing adhesion forces between the release film and the cured resin.[29] The printed structure remained stable even at a high printing speeds. Besides, adding an additional flexible film between the LCD screen and the release film effectively reduces the separation forces between the cured resin and the release film.[35] However, the deformation of the release film remains in the printing process, and the printing accuracy has not been studied. At the same time, we found no research directly examining the combined effect of the LCD screen and release film, ignoring how deformation of the release film could affect the printing accuracy. All in all, increasing the adhesion force between the LCD screen and release film to counteract the force between the release film and the cured resin can reduce the deformation of the release film during printing. Consequently, improving the printing accuracy at the microscale is worthy of further discussion and research.

As the adhesion between the LCD screen and the release film as well as the deformation of the release film are critical for printing accuracy, it's important to make the bond between the LCD screen and the release film stronger and keep the release film from bending. Here, we proposed using an immobilized release film to enhance the printing accuracy of microscale printing for microfabrication. Briefly, by applying transparent double-sided adhesive tape between the LCD screen and release film, the movement and deformation of the release film can be reduced, the vertical accuracy in the process of microscale 3D printing can be improved, and the error rate in height can be reduced from 20% to 5%. In addition, we found that during the printing process, the UV light of the LCD printer is slightly divergent with a divergent angle of about ±10°. Through the study of the printing effect under different layer heights, it was found that when the layer height was set to 20–30 μm, the printed micromold is consistent with design features in terms of size and side structure. At the same time, we discovered that the divergent light of the UV lamp also affects the horizontal accuracy of the mold. When printing a

ridge structure, the actual size is slightly smaller than the design size; when printing a hollow structure, it is slightly larger. Moreover, a microstructure of less than 30 μm width was obtained. Besides, the reproducibility of the immobilized release film across different resins was confirmed. Then, we printed microfluidic chips with different structures and concentration gradient generation molds with a minimum cross section of 204 μm. Finally, we used the printed mold to fabricate a PDMS chip in the study of silicosis and the preventive effect of NAC in silicosis. Moreover, the mechanism of the preventive effect of NAC was studied.

Materials and methods

More detailed information on the Materials and methods used can be found in the ESI.†

Immobilizing the release film on the LCD screen

According to the manufacturer's manual, the resin tank is just placed on the LCD screen without any further treatment. The gap between the LCD screen and release film varied during layer printing. To eliminate this unstable factor that influences the printing efficiency, we used a transparent double-sided tape (3M, 55256, 50 μm thickness) to immobilize the smooth release film on the LCD screen. To ensure strong adhesion and good imaging quality, the transparent double-sided tape should be applied careful without any bubbles or contaminants. The immobilization of the release film on the LCD screen ensured the printing accuracy while printing.

Microscopy and image analysis

An inverted microscope (Olympus, CKX53) with a charge-coupled device camera (Olympus, DP73) and a mercury lamp (Olympus, U-RFL-T) were used to acquire the optical and fluorescent images. Software Image-Pro Plus 6.0 (Media Cybernetics, Silver Spring, MD) and SPSS 12.0 (SPSS, Inc.) were utilized for image and data analysis, respectively. The results including the error bars are presented as the mean ± standard deviation (SD).

Results and discussion

Accuracy characterization with immobilized release film

To explore the potential of high-precision printing by an LCD-based 3D printer in microfabrication, an LCD-based 3D printer (Anycubic, Photon M3 Plus) was chosen. It was observed that, by default, the release film is frosted on one side to facilitate release in large mold printing. To obtain a smooth top surface of the micromolds, the frosted release film was replaced with a smooth release film. According to the manufacturer's manual, the resin tank is just placed on the LCD screen without any further treatment. An unexpected gap and a weak adhesion force between the LCD screen and release film was observed during printing (Fig. 1A). To verify whether the gap and weak adhesion force between the LCD screen and release film influences the printing accuracy or not, we printed molds using the printer with the default gap (weak adhesion force between the LCD screen and release film) and a 150 μm gap (no adhesion between the LCD screen and release film). The results in Fig. 1B show that the printed height was not consistent with the designed height. Besides, when the gap between the LCD screen and release film was increased to 150 μm, the height of the printed microstructure was significantly reduced during printing. Moreover, with the gap increased, the error rate between the designed height and the printed height was increased from about 20% to 40% or more (Fig. 1C). It is assumed that the vertical accuracy is influenced by the free motion of the release film during the upward movement of the printing platform. To eliminate the gap and enhance adhesion between the LCD screen and release film, we proposed immobilizing the release film on the LCD screen using transparent double-sided tape, as shown in Fig. 1D.

To determine whether the printing accuracy can be improved with the immobilized release film or not, the micromolds printed by the LCD printer were thoroughly studied. First, the UV intensity was tested. The UV intensity without transparent double-sided tape was 11.13 ± 1.678 μW cm^{-2}, while the UV intensity with transparent double-sided tape was 10.82 ± 1.376 μW cm^{-2}. The change was not obvious and does not affect the curing of the resin. After that, the accuracy in the vertical direction with a specific layer height was examined. The layer height was controlled by the *Z*-axis screw rod and stepping motor. The cooperation of the Z-axis screw rod and stepping motor determined the resolution in the vertical direction. According to the manufacturer's instructions, a 50 μm layer height was inspected first. Structures with a 204 μm width (6 pixels in the LCD screen) and different heights (from 50 μm to 500 μm with a step size of 50 μm, *i.e.*, from 1 to 10 layers) were designed and printed. Through the unique design, the LCD screen with six pixels can be set to pass or obstruct UV light. When the UV light was obstructed by the LCD screen, a hollow structure on the mold was achieved. On the contrary, when the UV light passed through the LCD screen, a ridge structure on the mold was obtained. Furthermore, to maintain the desired fine structure, a resin platform measuring 10 000 μm in length and width and 1000 μm in height, was designed (Fig. S1†). With the resin platform, the fine structure can be preserved completely. In the side view of the model, the ridge and hollow structures were printed layer by layer with uniform layer height. Statistical data show that the heights of the hollow or ridge structures have a good correlation with the number of layers (Fig. 1E). Furthermore, the error rate of the printed structure on molds with different layers was reduced to 5% except for single layer printing (Fig. 1F). These results demonstrate that immobilizing the release film with transparent double-sided tape can improve the printing accuracy and reduce the printing error rate.

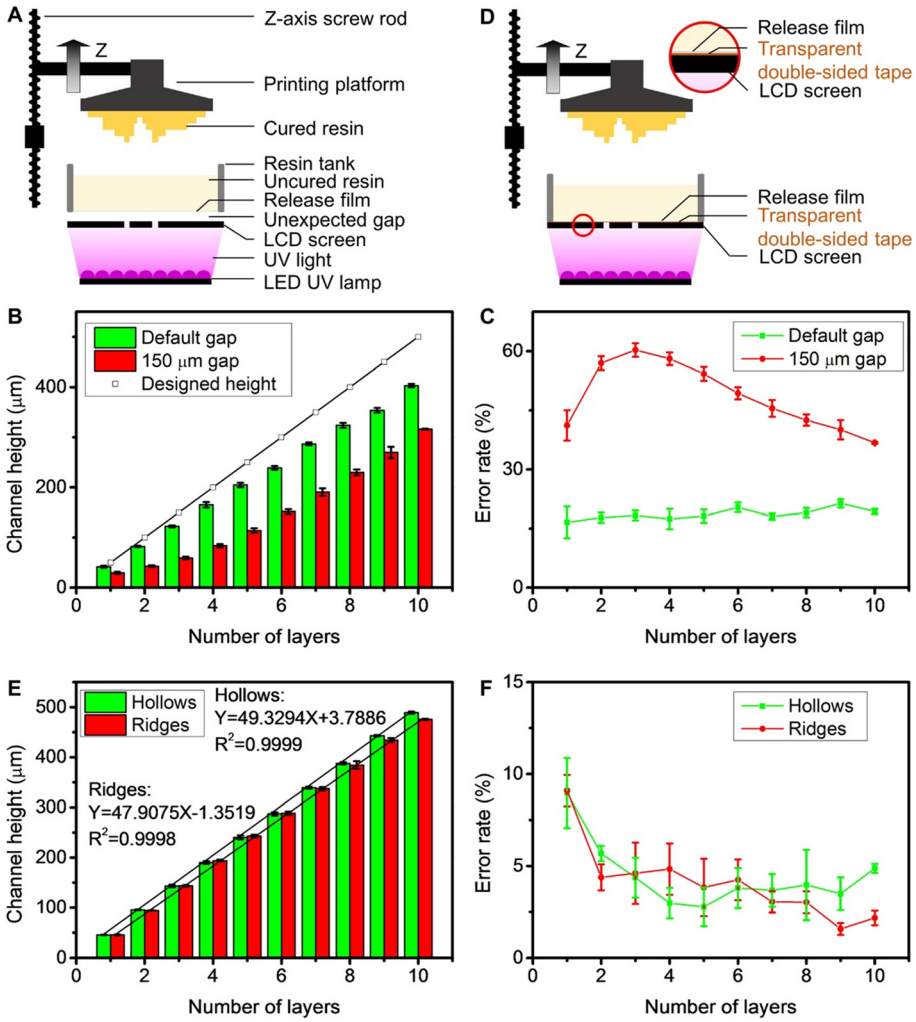

Fig. 1 Microstructure printing using an LCD-based 3D printer. (A) An illustration of the main components of the LCD-based 3D printer. There is an unexpected gap between the release film and LCD screen. (B) Channel height of the printed structure on molds with different layers under the default gap and 150 μm gap. (C) Error rate of the printed structure on molds with different layers under the default gap (weak adhesion force between the LCD screen and release film) and 150 μm gap (no adhesion between the LCD screen and release film). (D) An illustration of the LCD-based 3D printer with release film immobilized by transparent double-sided tape. (E) Channel height of the printed structure on molds with different layers using an LCD printer with an immobilized release film. (F) Error rate of the printed structure on molds with different layers using an LCD printer with an immobilized release film.

Layer height optimization

Furthermore, different layer height settings of the printing process were investigated. Molds with different heights (from 100 μm to 1000 μm with a step size of 100 μm) were designed and sliced with different layer heights (from 10 μm to 100 μm with a step size of 10 μm) to study the printing effect under different layer heights. As shown in Fig. 2A, the structure can be fabricated and perfect alignment was maintained between the upper and lower layer. Meanwhile, the height of the structure showed a good relationship with the layer height (Fig. 2B). However, it was observed that the error rate of the printed mold with 10 μm layer height was significantly high at 30%. This may be because the extremely small layer height set reaches the limit of the equipment, which can lead to an increase in error and error rate.

Furthermore, it is obvious that as the layer height increases, the unequal width between the top and bottom of a single layer becomes more visible (Fig. 2A and D). This phenomenon can be observed when the layer height is larger than 30 μm. It is supposed that this phenomenon was determined by the inherent characteristic of the 3D printer, *i.e.*, the UV light source and LCD screen co-induced this special phenomenon. Briefly, the UV light source was composed of 40 UV lamps. The UV light emitted by lamps was not parallel. According to the angle of the cured resin under different layer heights, it is assumed that the divergent angle of the UV light was about ±10° (red line in Fig. 2D). After the divergent UV light passes through the mask presented by the LCD screen, it acts on the resin in three different states: all pass, all block, and divergence (Fig. 2E). In detail, when blocked by the LCD screen, the UV light was unable to pass the screen and cure the resin. Therefore, the

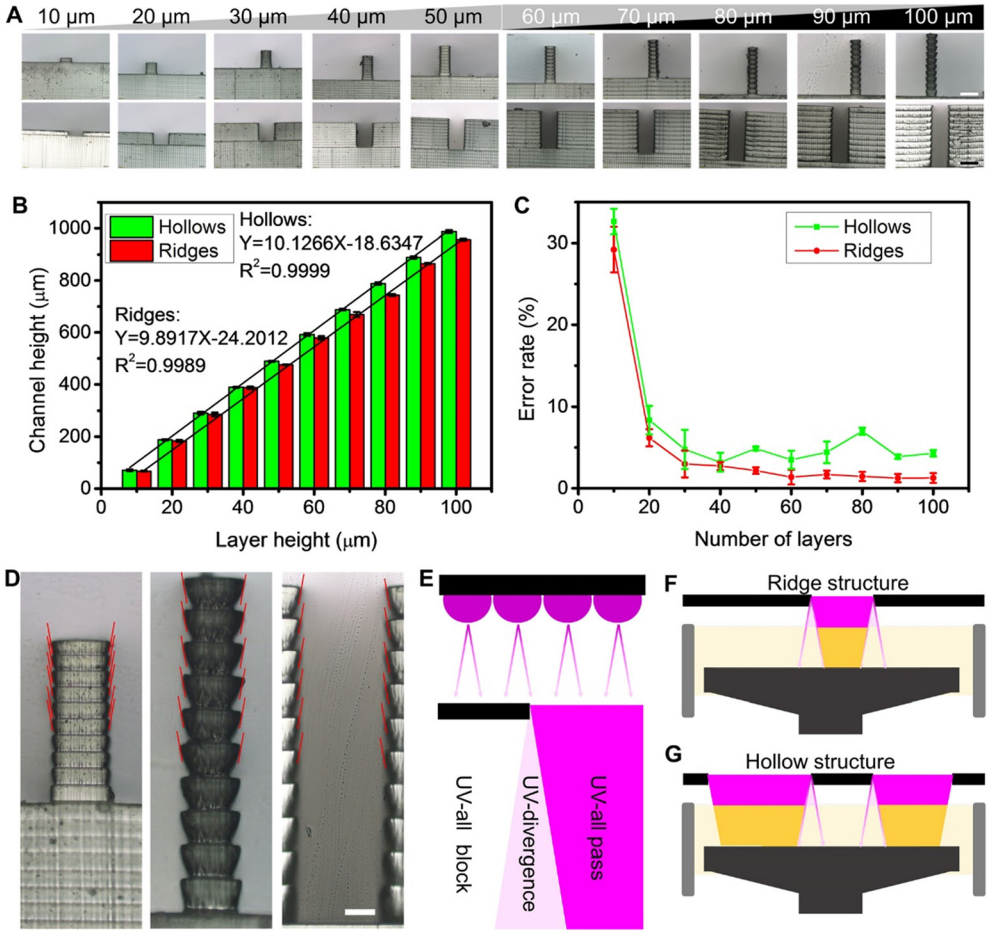

Fig. 2 Layer height optimization of the LCD-based 3D printer. (A) The side views of the printed structures with different layer heights. Scale bars: 300 μm. (B) Channel height of the printed structure on molds with different layer heights. (C) Error rate of the printed structure on molds with different layer heights. (D) The side view of the printed ridge structure with special features. The red line was assumed to be the divergent angle of UV light. (E) An illustration of the different divergent UV light action. (F) An illustration of the ridge structure fabrication. (G) An illustration of the hollow structure fabrication. Scale bars: 100 μm.

resin will not be cured in the all block state. In the all pass situation, the UV light can pass through the LCD screen and reach the resin tank to cure the resin. Hence, the resin can be cured by UV light in the all pass state. Notably, at the edge of the pattern of the LCD screen, the UV light diverged, and the intensity of UV light decreased after the divergent UV light pass. The resin was unable to be cured by the UV light with reduced intensity in the divergent state (Fig. 2E). The different states of UV light can be used to explain the difference of the unequal width between the top and bottom of a single layer. As shown in Fig. 2F and G, under the irradiation of the divergent UV light, with the increase in the layer height, the resin was cured with a unique shape. The unique shape of the model may be used in some specific fields. However, it is inappropriate when used as a mold in device fabrication. Hence, to maintain an acceptable parameter of layer height in 3D printing, we inspected the ridge and hollow structures with different layers under different layer height settings (Fig. S2†). The results revealed that the height of the mold showed a good relationship with the layer number. To maintain a good printing effect, the layer height was set between 20 and 30 μm and the 25 μm layer height was systemically studied (Fig. S3†).

Horizontal accuracy characterization

In Fig. 2F and G, we can find that the printed width may deviate from the design width. To inspect the difference between the printed width and the design width, exquisite molds were designed to achieve an LCD screen with 1–10 pixels ON or OFF to pass or block UV light (Fig. 3A). With the resin platform, the fine structure can be completely preserved (Fig. 3B). It can be seen that the desired structure was printed with clear edges and uniform width (Fig. 3C). Moreover, the structure can be utilized to make PDMS by the molding method (Fig. 3D). Statistical data showed that the entire width of the hollow or ridge was uniform (Fig. 3E). Meanwhile, the structure width showed a good relationship with the number of pixels in the LCD screen. By the molding method, it is easy to transform the complete smooth ridge or hollow structure to PDMS as a channel or pillar with high accuracy (Fig. 3F). However, it is noted that the width

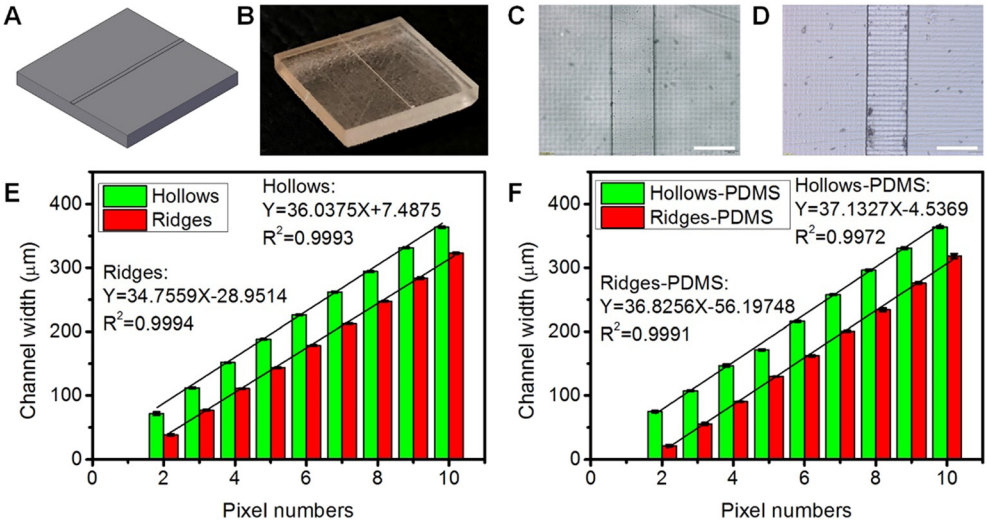

Fig. 3 Horizontal accuracy characterization of the LCD-based 3D printer. (A) Scheme of the printed model used in horizontal accuracy characterization. (B) Photo of the printed model. (C) The printed ridge structure on the model. (D) The structure on PDMS fabricated by the printed model. (E) Channel width of the printed structure on the mold. (F) Channel width of the structure on PDMS. Scale bars: 300 μm.

of the hollow structure was larger than the theoretical width, while the width of the ridge structure was smaller than the theoretical width. This may be caused by the inherent properties of the LCD-based 3D printer. As shown in Fig. 2F, while fabricating the ridge structure, the width of the UV light that can cure the resin was reduced, which causes the width of the ridge structure to decrease. While fabricating the hollow structure, the width of the UV light that cannot cure the resin was increased, which caused the width of the hollow structure to increase (Fig. 2G). More importantly, it is hard to get a ridge or hollow structure using an LCD screen using only one pixel. This may be due to the resin properties and resin post-treatment process. It is difficult to rinse the uncured resin from the small gap, and the tiny cured resin can be easily flushed away. The width of the narrowest ridge structure of the mold was about 40 μm, which was achieved when two pixels were applied to the LCD screen as the dynamic mask (Fig. 3E). When transforming the ridge structure on the mold to a channel in a PDMS chip, the size can be less than 30 μm (Fig. 3F). The micro-sized channel exhibits wide prospects in applications, such as reagent transferring and cell culture.

Reproducibility of the immobilized release film across different resins

Next, to verify the reproducibility of the enhanced printing accuracy across different resins, different types of resin with different properties were obtained from different manufacturers (Table S1†). Molds with different heights were printed with a layer height of 50 μm and 25 μm, respectively. Meanwhile, different print modes by the printer with default gaps or immobilized release films were used. As shown in Fig. S4–S6,† it can be seen that the error rate can be significantly reduced when the immobilized release film is used. These results show that the printing method using an immobilized release film has versatility and reproducibility in improving the printing accuracy with different resins.

Immobilization of the releasing film with multilayer transparent double-sided tape

Besides, to further study whether the print effect was affected by the adhesive tape's thickness, multilayer transparent double-sided tape was applied between the LCD screen with the release film. Briefly, three-layer double-sided adhesive tape (thickness: 150 μm in total) was utilized, and molds with different height were printed with a layer height of 50 μm. Meanwhile, exquisite molds with different width were printed. After three-layer double-sided adhesive tape was applied, the UV intensity was 11.30 ± 1.6525 μW cm^{-2}, and there is no difference in the UV intensity with/without double-sided adhesive tape. From the results in Fig. S7,† we can see that the channel height is in a good relationship with the number of layers, and the error rate was below 5%. These data show that the thickness of the adhesive tape will not affect the print accuracy in the vertical direction. However, the channel width of the hollow structure was much larger than the theoretical width, while the channel width of the ridge structure was much smaller than the theoretical width. This may be caused by the distance between the LCD screen and release film. Under the effect of divergent UV light, as the distance between the LCD screen and the release film increases, the deviation between the printed width and the theoretical width also increases.

Sophisticated structure fabrication

Afterwards, more complex structures, such as a right-angled triangle, square, pentagon, hexagon, and circle were designed and printed. To maintain the best structure, all of these structures were designed and printed on the same resin platform as mentioned above. After printing and washing, all

the structures were obtained. As shown in Fig. 4A, we can see that the pattern shape can be maintained after printing. Although the size of the right-angled triangle was reduced because of the inherent characteristic of the 3D printer mentioned above, the shape of the right-angled triangle was preserved. The results indicated that it is suitable for sophisticated structure fabrication.

Besides, a model with a hollow pipeline was designed and printed by our 3D printer. It can be seen from Fig. 4B and C that the hollow pipeline was designed in a cuboid model measuring 20 000 μm in length, 10 000 μm in width and 2000 μm in height, while the cross section of the hollow pipeline was a rectangle with a width from 102 to 1020 μm with a step size of 102 μm and a height from 100 to 1000 μm with a step size of 100 μm. A single layer (20 000 μm, 10 000 μm and 25 μm in length, width and height) was set to close the hollow pipeline. The layer height was set as 25 μm in slicing. After printing and washing, the model reveals a clearly visible hollow pipeline in the side view (Fig. 4D). However, it is hard to confirm whether the hollow pipeline was unobstructed or not. To further characterize the hollow pipelines, red ink was applied to indicate the pipelines. As show in Fig. 4E, the hollow pipeline was unobstructed, while the edge length of the cross section was larger than 204 μm. It can be seen that while the pipeline was 102 μm in edge length of the cross section, only part of the pipeline can be obtained. This may be because of the properties of resins. The resin was highly viscous and hindered the post-washing of the model with a confined channel. Furthermore, the serpentine hollow pipeline with the cross section measuring 204 μm in width and 200 μm in height was obtained, as shown in Fig. 4F. Afterward, the direct printed chip with the classic structure of the concentration gradient generator containing two inlets and five outlets was designed and printed with a cross section measuring 204 μm in width and 400 μm in height (Fig. 4G). Moreover, the functional tests of the concentration gradient generator were conducted with methyl blue solution. As shown in Fig. S8,† a stable concentration gradient can be formed by the five outlets, which is consistent with the simulation results. The excellent precision in printing exhibited the unlimited potential of desktop LCD-based 3D printers in the microfluidic field.

Silicosis research

Silicosis is a most serious disease and has the highest number of cases among occupational diseases, especially in developing countries.[36] Due to the inhalation of silicon dioxide (SiO_2), SiO_2 is deposited on the surface of alveoli and hinders the physiological function of the lungs.[37] Exploring the pathogenesis and treatment of silicosis is crucial for understanding silicosis. Here, we use a microfluidic chip prepared by the desktop LCD-based 3D printer to establish a silicosis model and investigate the pathogenesis of silicosis.

The microfluidic chip consisted of a cell culture layer with a main chamber (87 000 μm, 1000 μm and 150 μm in length, width and height) for cell culture and two channels (each measuring 5000 μm in length, 200 μm in width and 150 μm

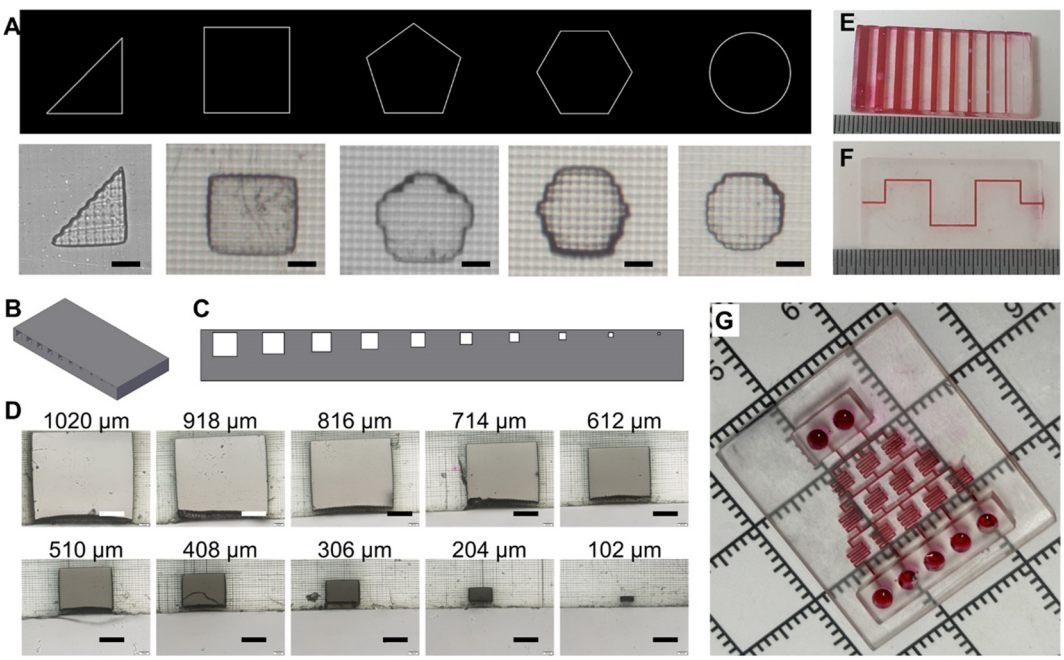

Fig. 4 Sophisticated structure fabrication of the LCD-based 3D printer. (A) Scheme of the printed sophisticated structures. Scale bar: 100 μm. (B) Scheme of the model with different hollow pipelines. (C) Side view diagram of the model with different hollow pipelines. (D) The side view of the printed model with different hollow pipelines. Scale bars: 200 μm. (E) Photo of the printed model with different hollow pipelines. Red ink was filled in the pipelines. (F) Photo of the printed model with a serpentine hollow pipeline. Red ink was filled in the pipeline. (G) Photo of the printed concentration gradient generator. Red ink was filled in the channel.

in height) for connecting with an inlet and an outlet, a thin PDMS layer and a glass layer for support (Fig. 5A and B). To conveniently fabricate the PDMS chip, an integrated mold with 12 of the same patterns was designed to fabricate 12 separate PDMS chips in one experiment. Meanwhile, a fence of 4 mm height was designed to prevent the overflow of the pre-solidified PDMS. After printing, the integrated mold was glued to the glass to prevent thermal deformation during the prolonged baking process (Fig. 5C). Then, well-mixed pre-solidified PDMS was poured onto the mold. After degassing and baking, the PDMS replica is peeled off from the mold, and 12 independent PDMS chips were separated using a cutter, and the inlet and outlet were punched by a needle. Then, the independent PDMS chip was bonded onto a glass slide with a thin layer of PDMS for later use (Fig. 5D).

Human pulmonary alveolar epithelial cells (HPAEpic) were used in our experiment to construct the *in vitro* silicosis model. Before cell culture, the chamber was pretreated by collage I (200 μg mL^{-1}) to enhance the cell adhesion. The untreated PDMS was not suitable for cell adhesion and culture. Then, cells were introduced into the chip from the inlet and cultured in the main chamber. After the cells were confluent, media with different concentrations of SiO_2 were introduced into the chamber to obtain the silicosis model. As shown in Fig. 5E, under low concentration SiO_2, the cells remained in a good state. However, under high concentration SiO_2, the cells shrank and detached from the surface of the culture chamber. With FDA/PI double staining, we can see that with the increase of the concentration of SiO_2, the dead cells were increased. Statistical data showed that the cell viability was higher than 95%, while the concentration of SiO_2 was below 500 μg mL^{-1}. When the concentration of SiO_2 was 1000 μg mL^{-1}, the cell viability was 84.03% ± 2.576% only (Fig. 5F). The results from the simulation revealed that high concentrations of SiO_2 can damage pulmonary alveolar epithelial cells.

N-Acetylcysteine (NAC) is an antioxidant amino acid derivative, which can reduce cell damage, promote complete tissue restoration and improve patient survival rate.[38] To study the preventive effect of NAC, cells were treated with 4 mM NAC for three hours before SiO_2 simulation. The results revealed that NAC can effectively alleviate the damaging effect of SiO_2 on cells (Fig. 6A and B). To determine the mechanism of the preventive effect of NAC, we investigated the level of reactive oxygen species (ROS) and cell apoptosis.[39] ROS are considered as the pivotal signaling molecules in many physiological processes and are usually overproduced in various tissues under stimulation.[40] Overproduction of ROS may disrupt cellular homeostasis, cause cell apoptosis, and lead to diseases. The thiol group of NAC has antioxidant properties, which can reduce the level of ROS and cell apoptosis.[41] The results from simulation of SiO_2 revealed that exposure to SiO_2 significantly increased the ROS and apoptosis levels in the cells (Fig. 6C and E). With the

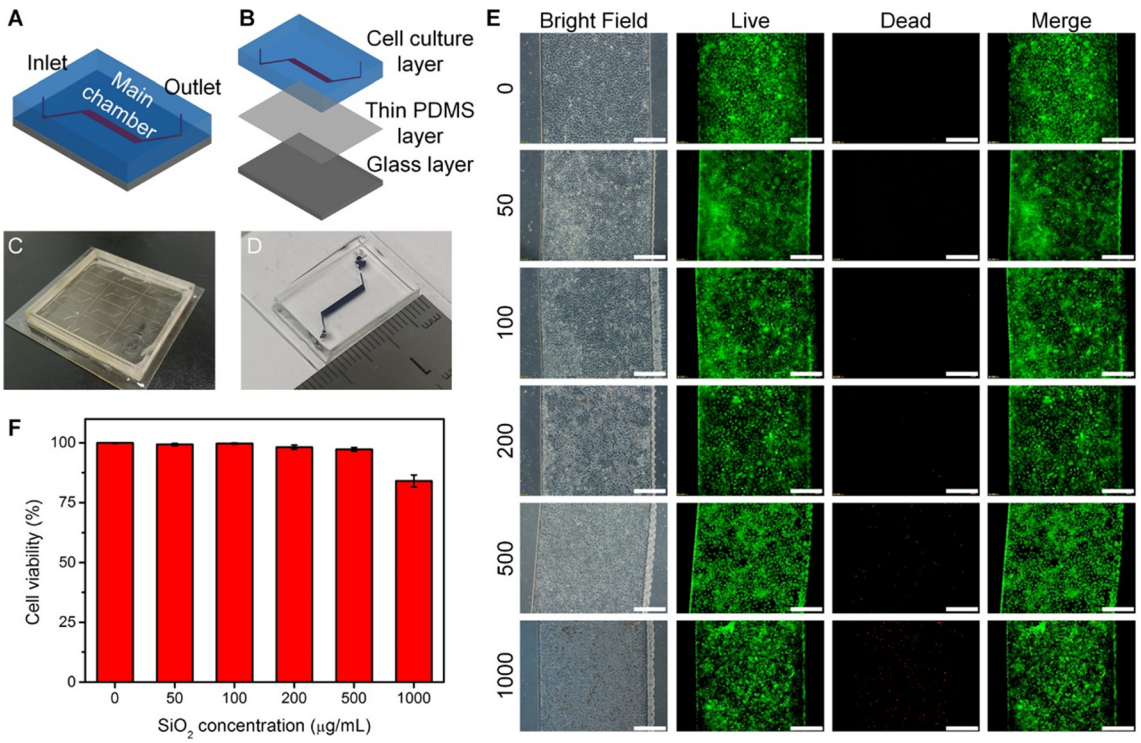

Fig. 5 Silicosis model construction. (A) The illustration of the microfluidic chip used in silicosis model construction. (B) The composition of the microfluidic chip used in silicosis model construction. (C) The integrated mold used in microfluidic chip fabrication. (D) The photo of the microfluidic chip used in silicosis model construction. (E) FDA/PI double staining of the silicosis model with different concentrations of silicon. (F) Cell viability of the silicosis model with different concentrations of silicon. Scale bars: 300 μm.

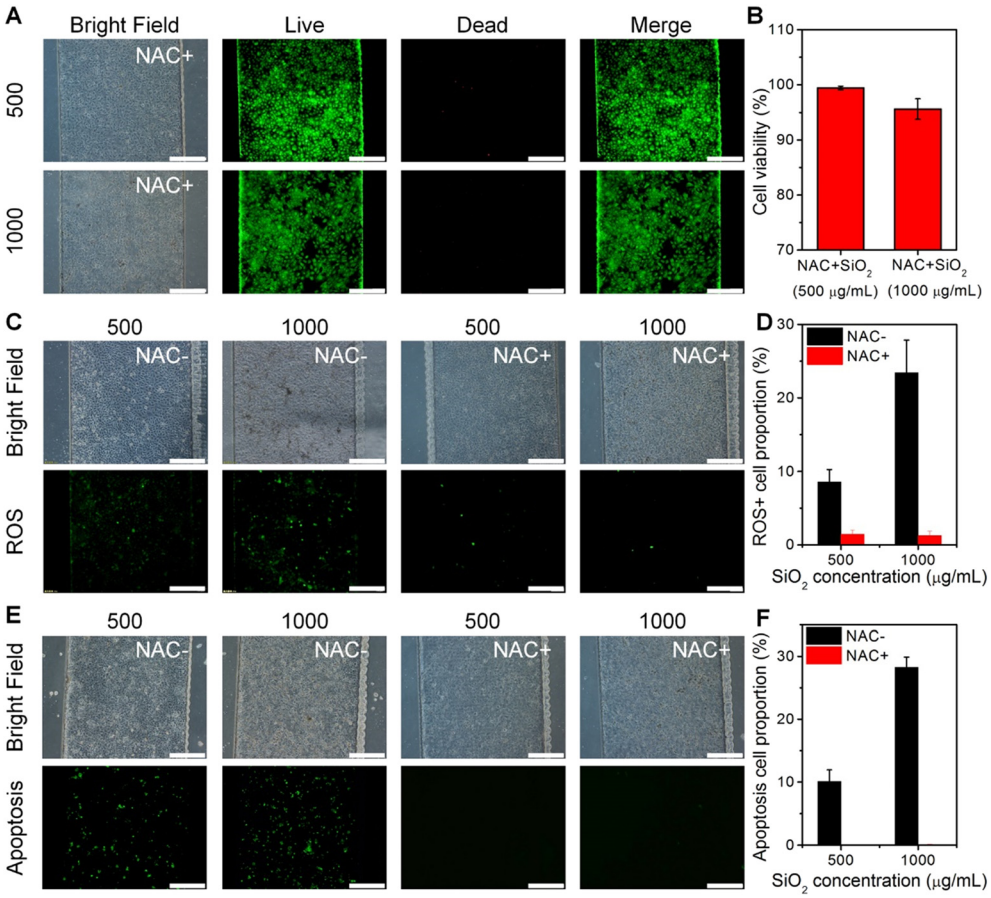

Fig. 6 The mechanism study of the preventive effect of NAC. (A) FDA/PI double staining of the silicosis model with NAC treatment. (B) Cell viability of the silicosis model with NAC treatment. (C) ROS characterization of the silicosis model with/without NAC treatment. (D) Quantitative analysis of the ROS level of the silicosis model with/without NAC treatment. (E) Apoptosis characterization of the silicosis model with/without NAC treatment. (F) Quantitative analysis of the apoptosis level of the silicosis model with/without NAC treatment. Scale bars: 300 μm.

treatment of NAC, the ROS and apoptosis level of the cells was significantly reduced. Statistical data showed that the treatment of NAC can effectively reduce the level of ROS and apoptosis (Fig. 6D and F). The extremely protective effect of NAC revealed that NAC can effectively maintain intracellular homeostasis and prevent silicosis. Furthermore, the experimental results have demonstrated the feasibility of using the chip prepared by the LCD-based 3D printer for pneumoconiosis research, showcasing potential in the field of biology and medical research.

Conclusion

In summary, we established a method whereby immobilizing the with release film can enhance the printing accuracy of an LCD-based 3D printer for preparing microfluidic chips. By applying transparent double-sided adhesive tape between the LCD screen and release film, the movement and deformation of the release film can be reduced, the accuracy of microscale 3D printing can be improved, and the error rate in height can be reduced from 20% to 5%. Through analyzing the relationship of the designed parameter of the model and the printed effect of the model, the divergent angle of UV light was determined to be about ±10°, and a smooth structure on the cross section was obtained when the layer height was set to 20–30 μm. Furthermore, a microstructure with a width below 30 μm can be printed. Besides, the reproducibility of the immobilized release film across different resins was confirmed. Utilizing the LCD printer, different complex structures were printed, and a hollow pipeline measuring 204 μm in width can be fabricated. Moreover, the application of this method in silicosis research in the medical field was conducted, and the mechanism of the preventive effect of NAC was explored. We believe that our fabrication technique with the immobilized release film will facilitate the development of microfluidic technology, expand the scope and application of microfluidics in the research and application of diverse fields, such as analytical biochemistry, pharmaceuticals, and medicine.

Data availability

The data supporting this article have been included as part of the manuscript and the ESI.†

Conflicts of interest

The authors declare that they have no known competing financial interests or personal relationships that could have appeared to influence the work reported in this paper.

Acknowledgements

This work was supported by the Natural Science Research Project of Anhui Educational Committee (2022AH050829), University-level Key Projects of Anhui University of Science and Technology (xjzd2020-20), Key Laboratory of Industrial Dust Deep Reduction and Occupational Health and Safety of Anhui Higher Education Institutes (AYZJSGXLK202201001), Anhui Provincial Natural Science Foundation (2108085QH358), Scientific Research Foundation for High-level Talents of Anhui University of Science and Technology (13200387), Annual Guiding Science and Technology Plan Project of Huainan (2022174), and National Natural Science Foundation of China (22204138). Human pulmonary alveolar epithelial cells (HPAEpiC) were provided by the School of Public Health of Southeast University.

References

1 D. M. Balazs and M. Ibanez, Widening the use of 3D printing A light-triggered fabrication method extends the functionality of printable nanomaterials, *Science*, 2023, **381**(6665), 1413–1414, DOI: **10.1126/science.adk3070**.

2 A. N. Hamilton, R. S. Mirmahdi, A. Ubeyitogullari, C. K. Romana, J. I. Baum and K. E. Gibson, From bytes to bites: Advancing the food industry with three-dimensional food printing, *Compr. Rev. Food Sci. Food Saf.*, 2024, **23**, e13293, DOI: **10.1111/1541-4337.13293**.

3 B. Ter Haar, J. Kruger and G. van Zijl, Off-site construction with 3D concrete printing, *Autom. Constr.*, 2023, **152**, 104906, DOI: **10.1016/j.autcon.2023.104906**.

4 K. Walia, A. Khan and P. Breedon, Polymer-Based Additive Manufacturing: Process Optimisation for Low-Cost Industrial Robotics Manufacture, *Polymers*, 2021, **13**(16), 2809, DOI: **10.3390/polym13162809**.

5 H. K. Balakrishnan, F. Badar, E. H. Doeven, J. I. Novak, A. Merenda, L. F. Dumée, J. Loy and R. M. Guijt, 3D Printing: An Alternative Microfabrication Approach with Unprecedented Opportunities in Design, *Anal. Chem.*, 2021, **93**(1), 350–366, DOI: **10.1021/acs.analchem.0c04672**.

6 R. F. Quero, G. D. da Silveira, J. A. F. da Silva and D. P. de Jesus, Understanding and improving FDM 3D printing to fabricate high-resolution and optically transparent microfluidic devices, *Lab Chip*, 2021, **21**(19), 3715–3729, DOI: **10.1039/d1lc00518a**.

7 F. Subirada, R. Paoli, J. Sierra-Agudelo, A. Lagunas, R. Rodriguez-Trujillo and J. Samitier, Development of a Custom-Made 3D Printing Protocol with Commercial Resins for Manufacturing Microfluidic Devices, *Polymers*, 2022, **14**(14), 2955, DOI: **10.3390/polym14142955**.

8 V. Gupta and B. Paull, PolyJet printed high aspect ratio three-dimensional bifurcating microfluidic flow distributor and its application in solid-phase extraction, *Anal. Chim. Acta*, 2021, **1168**, 338624, DOI: **10.1016/j.aca.2021.338624**.

9 G. K. M. Kabandana, T. Zhang and C. P. Chen, Emerging 3D printing technologies and methodologies for microfluidic development, *Anal. Methods*, 2022, **14**(30), 2885–2906, DOI: **10.1039/d2ay00798c**.

10 N. P. Macdonald, J. M. Cabot, P. Smejkal, R. M. Guijt, B. Paull and M. C. Breadmore, Comparing Microfluidic Performance of Three-Dimensional (3D) Printing Platforms, *Anal. Chem.*, 2017, **89**(7), 3858–3866, DOI: **10.1021/acs.analchem.7b00136**.

11 B. Gross, S. Y. Lockwood and D. M. Spence, Recent Advances in Analytical Chemistry by 3D Printing, *Anal. Chem.*, 2017, **89**(1), 57–70, DOI: **10.1021/acs.analchem.6b04344**.

12 J. T. Yu, J. Zhu, L. L. Chen, Y. H. Chao, W. S. Zhu and Z. C. Liu, A review of adsorption materials and their application of 3D printing technology in the separation process, *Chem. Eng. J.*, 2023, **475**, 146247, DOI: **10.1016/j.cej.2023.146247**.

13 H. Shafique, V. Karamzadeh, G. Kim, M. L. Shen, Y. Morocz, A. Sohrabi-Kashani and D. Juncker, High-resolution low-cost LCD 3D printing for microfluidics and organ-on-a-chip devices, *Lab Chip*, 2024, **24**(10), 2774–2790, DOI: **10.1039/d3lc01125a**.

14 H. Gong, B. P. Bickham, A. T. Woolley and G. P. Nordin, Custom 3D printer and resin for 18 μm × 20 μm microfluidic flow channels, *Lab Chip*, 2017, **17**(17), 2899–2909, DOI: **10.1039/c7lc00644f**.

15 Z. D. Yu, X. Q. Li, T. X. Zuo, Q. L. Wang, H. Wang and Z. Y. Liu, High-accuracy DLP 3D printing of closed microfluidic channels based on a mask option strategy, *Int. J. Adv. Des. Manuf. Technol.*, 2023, **127**, 4001–4012, DOI: **10.1007/s00170-023-11769-4**.

16 X. H. Wang, J. H. Liu, Y. Zhang, P. M. Kristiansen, A. Islam, M. Gilchrist and N. Zhang, Advances in precision microfabrication through digital light processing: system development, material and applications, *Virtual and Physical Prototyping*, 2023, **18**(1), e2248101, DOI: **10.1080/17452759.2023.2248101**.

17 D. Chekkaramkodi, L. Jacob, C. M. Shebeeb, R. Umer and H. Butt, Review of vat photopolymerization 3D printing of photonic devices, *Addit. Manuf.*, 2024, **86**, 104189, DOI: **10.1016/j.addma.2024.104189**.

18 D. M. Tsai and S. T. Chuang, 1D-based defect detection in patterned TFT-LCD panels using characteristic fractal dimension and correlations, *Mach. Vis. Appl.*, 2009, **20**(5), 423–434, DOI: **10.1007/s00138-008-0136-0**.

19 M. D. Poskus, T. Wang, Y. X. Deng, S. Borcherding, J. Atkinson and I. K. Zervantonakis, Fabrication of 3D-printed molds for polydimethylsiloxane-based microfluidic devices using a liquid crystal display-based vat photopolymerization process: printing quality, drug response and 3D invasion cell culture assays, *Microsyst. Nanoeng.*, 2023, **9**, 140, DOI: **10.1038/s41378-023-00607-y**.

20 K. M. Leong, A. Y. Sun, M. L. Quach, C. H. Lin, C. A. Craig, F. Guo, T. R. Robinson, M. M. Chang and A. O. Olanrewaju, Democratizing Access to Microfluidics: Rapid Prototyping of Open Microchannels with Low-Cost LCD 3D

Printers, *ACS Omega*, 2024, **9**(45), 45537–45544, DOI: **10.1021/acsomega.4c07776**.

21 M. Ramasamy, B. Ho, C.-M. Phan, N. Qi, C. L. Ren and L. Jones, Inexpensive and rapid fabrication of PDMS microfluidic devices for biological testing applications using low cost commercially available 3D printers, *J. Micromech. Microeng.*, 2023, **33**, 105016, DOI: **10.1088/1361-6439/acf2a7**.

22 I. Roohani, A. Entezari and H. Zreiqat, Liquid crystal display technique (LCD) for high resolution 3D printing of triply periodic minimal surface lattices bioceramics, *Addit. Manuf.*, 2023, **74**, 103720, DOI: **10.1016/j.addma.2023.103720**.

23 M.-Y. Sim, J.-B. Park, D.-Y. Kim, H.-Y. Kim and J.-M. Park, Dimensional accuracy and surface characteristics of complete-arch cast manufactured by six 3D printers, *Heliyon*, 2024, **10**, e30996, DOI: **10.1016/j.heliyon.2024.e30996**.

24 X. J. Zhang, Y. Y. Liu, Y. Bao, Z. X. Zheng, J. Mi, Y. X. Tang, Q. W. Zhang and A. E. Oseyemi, Dimension compensation of printed master molds by a desktop LCD 3D printer for high-precision microfluidic applications, *Microchim. Acta*, 2024, **191**, 583, DOI: **10.1007/s00604-024-06654-0**.

25 H. Taylor, Rapid 3D printing at the curved surface of a liquid, *Nature*, 2024, **634**(8036), 1061–1062, DOI: **10.1038/d41586-024-03392-4**.

26 R. F. Quero, D. P. de Jesus and J. A. F. da Silva, Simple modification to allow high-efficiency and high-resolution multi-material 3D-printing fabrication of microfluidic devices, *Lab Chip*, 2023, **23**(16), 3694–3703, DOI: **10.1039/d3lc00356f**.

27 A. Vedhanayagam, M. Golfetto, J. L. Ram and A. S. Basu, Rapid Micromolding of Sub-100 μm Microfluidic Channels Using an 8K Stereolithographic Resin 3D Printer, *Micromachines*, 2023, **14**(8), 1519, DOI: **10.3390/mi14081519**.

28 M. G. A. Mohamed, H. Kumar, Z. J. Wang, N. Martin, B. Mills and K. Kim, Rapid and Inexpensive Fabrication of Multi-Depth Microfluidic Device using High-Resolution LCD Stereolithographic 3D Printing, *J. Manuf. Mater. Process.*, 2019, **3**(1), 26, DOI: **10.3390/jmmp3010026**.

29 J. J. Wu, J. Guo, C. H. Linghu, Y. H. Lu, J. Z. Song, T. Xie and Q. Zhao, Rapid digital light 3D printing enabled by a soft and deformable hydrogel separation interface, *Nat. Commun.*, 2021, **12**, 6070, DOI: **10.1038/s41467-021-26386-6**.

30 D. A. Walker, J. L. Hedrick and C. A. Mirkin, Rapid, large-volume, thermally controlled 3D printing using a mobile liquid interface, *Science*, 2019, **366**(6463), 360–364, DOI: **10.1126/science.aax1562**.

31 C. Rein, K. Kamranikia, R. Council, P. Pezeshkpour, F. Kotz-Helmer and B. E. Rapp, Scanning-Laser-Based Microstereolithography of Microfluidic Chips with Micron Resolution, *Adv. Mater. Technol.*, 2024, **9**(20), 2400047, DOI: **10.1002/admt.202400047**.

32 J. R. Tumbleston, D. Shirvanyants, N. Ermoshkin, R. Janusziewicz, A. R. Johnson, D. Kelly, K. Chen, R. Pinschmidt, J. P. Rolland, A. Ermoshkin, E. T. Samulski and J. M. DeSimone, Continuous liquid interface production of 3D objects, *Science*, 2015, **347**(6228), 1349–1352, DOI: **10.1126/science.aaa2397**.

33 L. Wu, Z. Dong, H. Du, C. Li, N. X. Fang and Y. Song, Bioinspired Ultra-Low Adhesive Energy Interface for Continuous 3D Printing: Reducing Curing Induced Adhesion, *Research*, 2018, **2018**, 4795604, DOI: **10.1155/2018/4795604**.

34 H. Wen, Z. Wang, M. X. Tan, Q. X. Sui, S. R. Xu, S. J. Mao, T. Y. Xiao, Q. Yuan, B. Yuan, Y. Wu and J. Liu, Rapid vat photopolymerization through a superamphiphobic interface, *Virtual and Physical Prototyping*, 2023, **18**(1), e2255018, DOI: **10.1080/17452759.2023.2255018**.

35 X. Q. Wu, C. J. Xu and Z. M. Zhang, Flexible film separation analysis of LCD based mask stereolithography, *J. Mater. Process. Technol.*, 2021, **288**, 116916, DOI: **10.1016/j.jmatprotec.2020.116916**.

36 M. Mu, B. Li, Y. J. Zou, W. Y. Wang, H. B. Cao, Y. J. Zhang, Q. X. Sun, H. M. Chen, D. Y. Ge, H. H. Tao, D. Hu, L. Yuan, X. R. Tao and J. H. Wang, Coal dust exposure triggers heterogeneity of transcriptional profiles in mouse pneumoconiosis and Vitamin D remedies, *Part. Fibre Toxicol.*, 2022, **19**, 7, DOI: **10.1186/s12989-022-00449-y**.

37 H. H. Tao, H. Zhao, D. Y. Ge, J. J. Liao, L. C. Shao, A. W. Mo, L. L. Hu, K. Y. Xu, J. Wu, M. Mu, B. Li, X. R. Tao and J. H. Wang, Necroptosis in pulmonary macrophages promotes silica-induced inflammation and interstitial fibrosis in mice, *Toxicol. Lett.*, 2022, **355**, 150–159, DOI: **10.1016/j.toxlet.2021.11.015**.

38 D. Mokra, J. Mokry, R. Barosova, J. Hanusrichterova, C. H. Huang and B. H. Jiang, Advances in the Use of N-Acetylcysteine in Chronic Respiratory Diseases, *Antioxidants*, 2023, **12**(9), 1713, DOI: **10.3390/antiox12091713**.

39 L. Zhang, Y. L. He, Q. Z. Li, X. H. Hao, Z. F. Zhang, J. X. Yuan, Y. P. Bai, Y. L. Jin, N. Liu, G. Chen, X. Yun and S. Q. Yao, N-acetylcysteine alleviated silica-induced lung fibrosis in rats by down-regulation of ROS and mitochondrial apoptosis signaling, *Toxicol. Mech. Methods*, 2014, **24**(3), 212–219, DOI: **10.3109/15376516.2013.879974**.

40 Y. Z. Tian, H. Y. Shi, D. J. Zhang, C. F. Wang, F. Zhao, L. Li, Z. S. Xu, J. T. Jiang and J. Z. Li, Nebulized inhalation of LPAE-HDAC10 inhibits acetylation-mediated ROS/NF-κB pathway for silicosis treatment, *J. Controlled Release*, 2023, **364**, 618–631, DOI: **10.1016/j.jconrel.2023.10.018**.

41 M. C. D. Tenório, N. G. Graciliano, F. A. Moura, A. C. M. D. Oliveira and M. O. F. Goulart, N-Acetylcysteine (NAC): Impacts on Human Health, *Antioxidants*, 2021, **10**(6), 967, DOI: **10.3390/antiox10060967**.